Probabilistic analysis of Linear Mode vs Geiger Mode APD FPAs for advanced LADAR enabled interceptors

George M. Williams and Andrew S. Huntington

Voxtel, Inc., 12725 SW Millikan Way, Suite 230, Beaverton, OR, USA 97005-1782
www.voxtel-inc.com

ABSTRACT

To meet evolving ballistic missile threats, advanced seekers will include a multi-modal imaging capability in which a passive single- or multi-band infrared focal plane array (FPA) shares a common aperture with an active laser radar (LADAR) receiver – likely, a photon-counting LADAR receiver that can resolve photon times of arrival with sub-nanosecond resolution. The overall success of such a system will depend upon its photon detection efficiency and sensitivity to upset by spurious detection events.

In the past, to perform photon counting functions, it has generally been necessary to operate near infrared (NIR) avalanche photodiode (APD) FPAs in Geiger Mode. Linear Mode APDs could not provide enough proportional gain with sufficiently low noise to make the photocurrent from a single photon detectible using existing amplifier technology. However, recent improvements in APDs, sub-micron CMOS technology, and concomitant amplifier designs, have made Linear Mode single-photon-counting APDs (SPADs) possible.

We analyze the potential benefits of a LADAR receiver based on Linear Mode SPADs, which include: 1) the ability to obtain range information from more than one object in a pixel's instantaneous-field-of-view (IFOV), 2) a lower false alarm rate, 3) the ability to detect targets behind debris, 4) an advantage in the endgame, when stronger reflected signals allow dark current rejection via thresholding, and 5) the ability to record signal intensity, which can be used to increase kill efficiency. As expected, multiple laser shots of the same scene improves the target detection probability.

Keywords: THAAD, laser radar, LADAR, missile seeker, missile defense, single photon counting, avalanche photodiode, APD

1. INTRODUCTION

Hit-to-kill missile interceptors are a major component of the United States missile defense strategy (Figure 1). The task of hypersonic interception requires a robust kill vehicle with a highly capable seeker. To address emerging threats, advanced seekers must have the ability to track multiple closely spaced objects (CSOs), cope with countermeasures, and perform mission critical target discrimination functions in a cluttered battlespace (Figure 2).

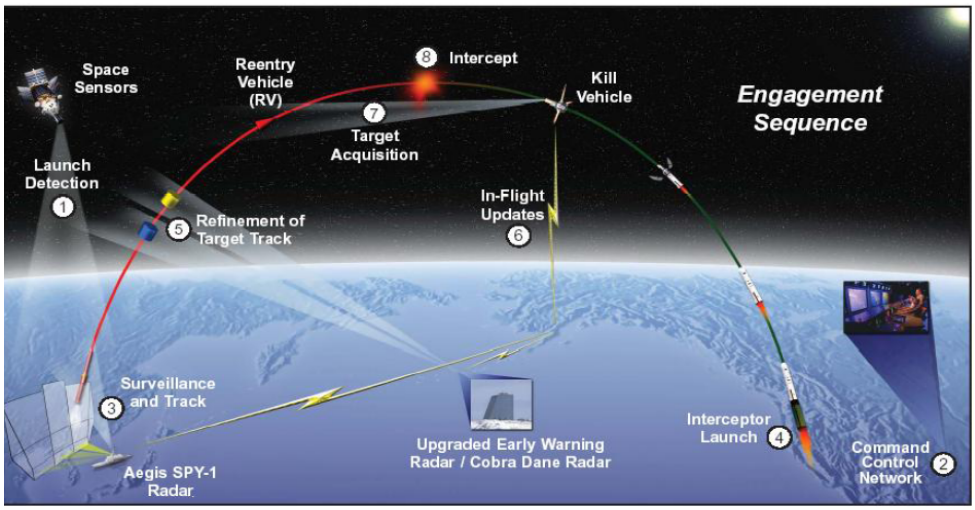

Figure 1: A representative BMDS weapon system. Courtesy of Missile Defense Agency: http://www.acq.osd.mil/mda/.

The effectiveness of current generation hit-to-kill defensive weapons with single-color passive IR seekers can be improved upon by adding an active LADAR imager.[1] The addition of a high-resolution 3-D imaging

capability improves the seeker's ability to collect data about a threat cloud's structure and the flight characteristics of its components. In this manner, dual-mode seeker architectures reduce BMD seeker systems' vulnerability to foreseeable countermeasures.

For seeker applications, LADAR FPAs based upon Geiger Mode SPADs have been demonstrated.[2] Additionally, Linear Mode SPADs are being developed[3] that show considerable promise over their Geiger Mode counterparts for BMD seeker applications.

Here, we are interested in providing an analysis of the performance differences between the two types of APD-based LADAR receiver. Our analysis builds upon a heuristic overview of hit-to-kill missile defense in the 21st Century as presented by LaCroix and Kurzius,[4] which serves as a useful platform for sensor tradeoff analysis.

1.1 Employment of the seeker

In general, a missile defense system interconnects an assembly of sensors and weapons. The sensors include space-based passive IR imagers that detect launches, ground-based tracking radar, and both passive and active imagers on the weapons themselves. In a typical operational scenario for an 'upper tier' missile defense system, the enemy ballistic missile launch is detected by an overhead sensor which cues the missile defense system. Interception of the warhead in its re-entry vehicle (RV) is attempted following burnout of its motor. During this time, the RV moves on an approximately parabolic path with an apogee of up to several hundred kilometers.[5] The warhead is accompanied on this trajectory by decoys and debris, which complicate identification of the warhead within the threat cloud (see Figure 2). Since the distance between the ground-based fire control radar and the threat cloud is long, objects within the threat cloud cannot be adequately resolved by radar alone. However, the trajectory of the threat cloud can be projected from radar data, permitting commitment of interceptors and prediction of the threat's impact point. The command, control, battle management and communications (C^2BMC) element of the missile defense system directs one or more interceptors to engage the threat at a point on its trajectory well away from the estimated impact point.

The interceptor is initially directed to the threat cloud by ground-based radar. However, imperfect guidance of the interceptor – as well as radar tracking errors – cause the kill vehicle (KV) to be released within a roughly spherical zone of uncertainty in the vicinity of the threat called the "handover basket". Within the handover basket, it is the role of the KV's seeker to autonomously detect the target within the threat cloud against the background of space, and maneuver to correct the error in the KV's intercept trajectory.

Various systematic errors conspire to place the KV and its target on non-intercept trajectories. These systematic errors may include timing errors, launch attitude alignment errors, navigation system errors, booster burn time variations, tracking sensor alignment errors, computational limitations, seeker alignment errors and more. Because of these errors, the KV will not initially have the correct position and velocity for an intercept. Since the systematic errors are generally uncorrelated, they may be summed in quadrature to accommodate all possible combinations and then assigned exclusively to the target as the handover error.

Seekers currently must correlate the 3-D target object map (TOM) generated by ground-based radar with the 2-D image from a passive IR sensor. Addition of 3-D LADAR functionality in a dual-mode seeker improves on the seeker's ability to match what it sees to the radar data. However, since radar and satellite target handoff baskets are large in angle space, the passive IR FPA of a dual-mode seeker must be used to perform bulk filtering to reduce the number of objects, and generate a prioritized location map for the LADAR to interrogate.

The ability to collect 3-D data afforded by the LADAR increases kill probability by providing a 3-D-to-3-D correlation with the TOM. This becomes crucial in a cluttered battle space in which the passive IR sensor will likely see many more objects than are resolved by ground-based radar. The LADAR sequentially interrogates threat objects by illuminating them with multiple high power laser pulses. The return of the reflected light is timed on a pixel-by-pixel basis.

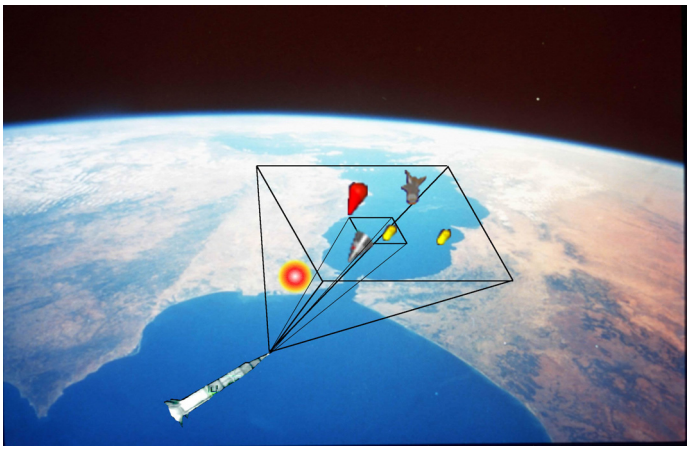

Figure 2: Illustration of terminal TBM engagement phase.

The resulting image is then sampled in snapshot mode, and 3-D angle-angle-range (AAR) information is generated. Processing of this data over multiple pulses allows separation of CSOs and extraction of micro-dynamic information used for target discrimination.

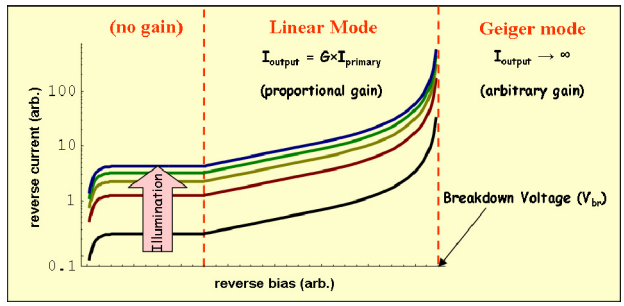

Figure 3: Schematic APD I-V curves showing the Linear Mode and Geiger Mode operating points.

By some estimates, the theater high altitude area defense (THAAD) KV must acquire its target at a range of at least 50 km to ensure a high kill probability.[6] Depending on the nature of the threat, the closing speed of the engagement may be as much as 10 km/s,[6] and assuming the threat cloud is acquired at a range of 50 km, the seeker will only have five seconds to pick the live warhead out of a battlespace cluttered with debris and decoys, and guide the kill vehicle to its aim point. Confounding this task is that throughout a majority of the engagement, the targets are unresolved, and that passive IR instruments are susceptible to simple countermeasures. For instance, the equilibrium temperature of a white balloon in sunlight at the engagement altitude is 227-241 K,[7] low enough to potentially defeat the passive IR FPA.[6]

Thus, sensitivity, speed, and timing accuracy requirements drive the dual-mode seeker design. Although early detection of objects will likely remain the primary responsibility of the passive IR FPA, a vital role of the LADAR camera is to augment the passive IR sensor in the search for CSOs (so to aide the IR seeker in accurately calculating temperature and emissivity measurements), provide shape information, and provide velocity estimates. In the terminal engagement phase, the RV must be hit squarely within a tight angular range, and the LADAR camera can assist with terminal guidance and aimpoint selection by taking high resolution snapshots of the RV at a high frame rate.[5]

Given the benefits of a dual-mode BMD seeker over the entirety of the engagement scenario, below we analyze the performance differences between SPAD-based LADAR FPAs in two different modes of operation: Linear and Geiger. Briefly, Linear Mode is operation below the APD's breakdown voltage for which the photocurrent is propotional to the received signal power, and Geiger Mode is operation above breakdown for which the photocurrent saturates at *any* level of received optical power (Figure 3). As will be developed, the two most important differentiating factors between Linear and Geiger APDs from the standpoint of LADAR applications are the Geiger APD's sensitivity to upset, and the possibility of rejecting dark current in a Linear receiver by thresholding.

1.2 Geometric optical design considerations

A typical KV is little more than a propulsion system with a seeker, computer, and communication device.[4] The seeker is configured differently for endo-atmospheric applications than for exo-atmospheric applications, but is generally located at or near the front of the KV and consists of an optical system, a detector suite, and image processing electronics. Today's technology can add high performance LADAR capability to a seeker with a relatively minor impact on mass and volume budgets.[5] A compact design requires that both passive and active signals be collected by a common aperture.

For the purposes of this discussion, we assume the seeker's dual-mode sensor suite consists of a passive IR FPA and a SPAD-based LADAR FPA. Wavelength-selective optics can then be used to separate the signals, with both channels imaged via relay lens assemblies onto their respective focal planes. The intermediate optics allow the two FPAs to have different fields of view (FOV).

During seeker design, a pixel's instantaneous field of view (IFOV) and frame rate must be appropriately balanced to accommodate the competing requirements for short-range resolution on one hand, and long-range sensitivity and total FPA FOV on the other. The seeker's FOV must be wide enough to include the threat cloud in the event of the largest likely handover error, [4] but at the same time, it must support accurate imaging and feature recognition during the final seconds of operation. Likewise, a slow frame rate with longer integration time is helpful in picking out distant targets, but a fast frame rate is required to capture details of target motion. These requirements are in opposition, and strongly commend a dual-mode seeker in which the passive IR FPA has a different FOV and frame rate than the LADAR FPA.[4]

Each FPA's FOV is determined by the physical size of the array and the optical system design. Knowing the f-number of the optical system, the aperture of the collection optics (d_o), and the pixel dimension (d_p), IFOV (ϕ_{pixel}) is obtained by simple geometry:

$$\phi_{pixel} = \frac{d_p}{d_o \times f_{\#}} . \quad (1)$$

The FPA's FOV is simply its pixel count multiplied by the IFOV of a single pixel. Practical passive IR FPAs are sized in the 128×128 to 512×512 pixel range with 20 µm and larger pixels. For a mid-wave infrared (MWIR) FPA with 30 µm pixels, a diffraction limited f/5 optic system with a 5-cm aperture results in a 120 µrad blur circle. The point spread function (PSF) is generally sampled with four pixels. When operating at 200 frames per second, a 5 ms dwell time is achieved in every frame.

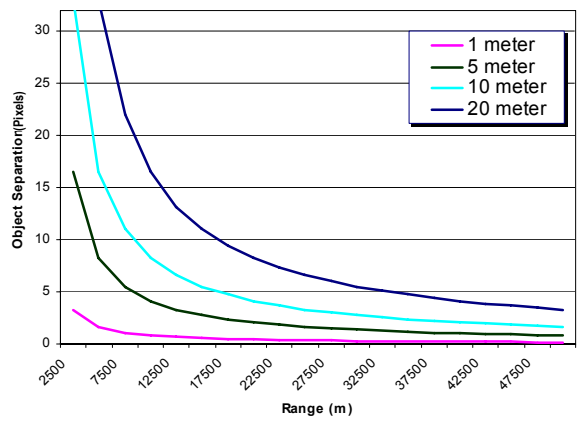

Figure 4: Number of pixels defining CSO separation for an 86 µrad IFOV LADAR seeker.

Ideally, the LADAR FPA should be optimized to complement the IR FPA, within the constraints of the technology. Geiger Mode SPADs have long existed, but the technology is more mature at the short wavelength end of the spectrum covered by silicon, than at the IR wavelengths which require compound semiconductor detectors. Although 1024×1024 silicon Geiger APD FPAs have been demonstrated,[8] silicon has only very weak response at the 1064 nm laser line commonly employed for LADAR illumination, and is not responsive to NIR laser illumination beyond 1100 nm. The few compound semiconductor Geiger APD arrays reported thus far are typically of much smaller format.

NIR photon counting in Linear Mode is a relatively new possibility. Linear Mode SPADs have been manufactured from silicon, although – as noted previously – silicon detectors have weak response at 1064 nm. Highly sensitive linear APDs manufactured from HgCdTe, InGaAs/InP, and InGaAs/InAlAs have also been reported that may be compatible with photon counting. In particular, electron avalanche HgCdTe APDs fabricated from 2.2 µm cutoff material have been recently demonstrated with excellent gain and excess noise characteristics.[9] These HgCdTe APDs should be capable of linear photon counting at 1064 nm, and up into the SWIR, when coupled with an appropriate low-noise amplifier.[9] The InGaAs-based linear APD technologies are derived from telecommunications receivers, and their performance is well documented. Conventional InGaAs-based APDs do not have the noise performance required to perform photon counting in Linear Mode, but promising results from newer impact-ionization engineered (I^2E) devices suggest that this can be achieved in the near future.[10]

Currently, HgCdTe and InGaAs SPAD FPA technology compatible with NIR operation is limited in size from 32×32 up to approximately 256×256 formats on an approximately 30 µm pixel pitch. Assuming f/7 optics and the same 5 cm aperture assumed for the passive IR FPA, a LADAR FPA with 30 µm pixels will have an 85.71 µrad IFOV – near its diffraction limit. Based on this geometry, an estimate of CSO separation in pixels versus target range is plotted in Figure 4. Such a LADAR FPA can resolve CSOs separated by 10 m, with 5 pixels or more resolution, at ranges up to 20 km.

Another requirement of the LADAR receiver is a frame rate that is matched, or exceeds, the pulse rate of the laser illuminator (e.g., 10 kHz). At a 10 kHz frame rate, 5 pulses on 20 different potential targets can be achieved within the 5 ms frame time of a 200 FPS passive infrared FPA. This allows a maximum line of sight (LOS) slew rate of 172 µrad/ms to ensure all five returns register in a single pixel.

The handover basket provided by the ground-based tracking radar, generally allows the LADAR to operate in a "range-gated" mode. Using time-of-flight to measure target distance, r, one relates the target range to bin number B as $r = r_1 + B\, r_0$, where r_1 is the spatial start of the LADAR's range gate and r_o is the temporal resolution of a time bin. The ground-based radar provides the seeker with a range uncertainty of approximately 60 m (0.4 µs time-of-flight for a laser pulse) to interrogate, so is some cases as few as 11 bits of range information must be stored per pulse to span that 60 m with 4.5 cm range bins (300 ps). However, for other scenarios, the on-chip time-of-flight data registers must have sufficient dynamic range to record laser echoes from targets as far away as 150 km (~1 ms), which can requires 23-bit time stamps.

1.3 Optical signal versus range

We stress that our aim is not to simulate the optical portion of this problem with great accuracy, but rather to compare the performance of Geiger versus Linear APDs, given an elementary model of the engagement. Accordingly, our

simplified treatment of optical signal versus range assumes a uniform target of constant aspect, a 'step function' beam profile, and neglects atmospheric scintillation.

Our starting point is the full angle beam divergence of the illuminating laser (θ), and its pulse energy E_{pulse}. This gives an illuminated spot size at range r of:

$$A_{spot} = \pi (r\,\theta/2)^2 \,. \tag{2}$$

In a system with constant beam divergence, the laser energy returned by the target will be proportional to r^{-4}. However, using the appropriate zoom optics, the LADAR system can adjust θ dynamically so as to keep A_{spot} constant at the target, resulting in energy returns proportional to r^{-2}. Hereafter, we assume that θ is dynamically adjusted based on the range to target, within certain bounds outlined below. We also assume at longer range that the laser beam-spot size at the target is large in comparison with the size of the target (i.e., the transmitted beam does not resolve the target) and the target depth (in the range direction) is small in comparison with the (longitudinal) coherence length of the transmitted beam.

The US MK-12A RV for the Minuteman intercontinental ballistic missile (ICBM) is conical, with a base diameter of 54.3 cm and a length of less than 181.3 cm.[11] The MK-12A represents a mature technology; a third-world RV threat will likely present a larger cross section. Although the cross-sectional area presented by the RV will vary depending upon the geometry of the engagement – not to mention the influence of surface features and target motion on reflectivity – we will make calculations based on a 1 m circular target for the sake of simplicity ($Area_{RV}$ = 0.79 m^2).

For our simulation, the tightest laser collimation we assume is $\theta_{min} = \phi_{pixel}$=86 µrad (which is just slightly higher than the diffraction limit for 1064 nm laser light and a 5 cm aperture). At a range of 11.7 km, a 1 m object will have an angular size equal to ϕ_{pixel}. Outside this range – and, therefore, throughout most of the engagement – the target is unresolved and the illuminated spot size is constant (with r^{-4} falloff in reflected energy). Inside this range, we assume that the beam is 'spoiled' in order to uniformly illuminate the entire 1 m target disk (with r^{-2} range dependence); however, because the area on the target imaged by a given pixel ($Area_{IFOV}$) increases as r^2, the average illumination collected by a pixel is actually constant inside 11.7 km. The widest useful value of θ is $\theta_{max} = \sqrt{2} \times 32 \times \phi_{pixel} = 3.9$ mrad – the FOV of the 32×32 pixel LADAR FPA. The beam divergence stops widening at 258 m, when $\theta = \theta_{max}$, and r^{-4} behavior resumes (see Figure 5).

Using the simplest geometric representation of beam propagation, at a target range r, the area density of photons delivered by a pulse of energy E_{pulse} within the cross section of the laser beam is:

$$\rho(r) = \frac{E_{pulse}}{h\,\nu \times A_{spot}} = \frac{E_{pulse}}{h\,\nu \times \pi \left(\frac{r\,\theta}{2}\right)^2} \,, \tag{3}$$

where $h\nu$ is the photon energy. For ranges at which the pixel's IFOV is larger than the target, the strength of the reflected return depends upon the cross-sectional area presented by the target ($Area_{RV}$); at ranges for which the target is larger than the pixel's IFOV, the strength of the reflected return depends upon the area of the target within the pixel's FOV ($Area_{IFOV}$). Light reflected from the target is assumed to be radiated isotropically, so the portion that is collected by camera optics of aperture d_o is simply the area ratio of the aperture ($Area_A$) to a sphere centered on the target. For a target of reflectivity R at range r, the average number of photons which impinge upon a pixel $\langle m \rangle_r$ is, for the resolved case:

$$\langle m \rangle_r = \frac{\rho(r) \times R \times Area_{IFOV}}{4\pi\, r^2} \times Area_A = \rho(r) \times R \times \frac{\pi}{64} \phi_{pixel}^2\, d_o^2 \qquad \text{for } Area_{IFOV} \le Area_{RV} \,, \tag{4a}$$

or for the unresolved case:

$$\langle m \rangle_r = \frac{\rho(r) \times R \times Area_{RV}}{4\pi\, r^2} \times Area_A = \rho(r) \times R \times Area_{RV} \times \frac{d_o^2}{16\, r^2} \qquad \text{for } Area_{IFOV} > Area_{RV} \,. \tag{4b}$$

The simplest treatment of signal photon statistics assumes that they obey Poisson's distribution, such that the probability of m photons arriving at the pixel is:

$$P_{Poisson}(m,r) = \frac{\langle m \rangle_r^m \exp\left(-\langle m \rangle_r\right)}{m!}. \tag{5}$$

In many cases of practical concern, laser speckle must be taken into account, in which case, the negative-binomial distribution is appropriate:[12]

$$P_{NB}(m,r) = \frac{\Gamma(m+M_r)}{m!\,\Gamma(M_r)} \left(1+\frac{M_r}{\langle m \rangle_r}\right)^{-m} \left(1+\frac{\langle m \rangle_r}{M_r}\right)^{-M_r}, \tag{6}$$

where $\Gamma(z) \equiv \int_0^\infty dt\, t^{z-1} \exp(-t)$ is the Euler gamma function, and M_r is Goodman's parameter representing the mean number of correlation cells at range r. The negative binomial distribution reduces to the Poisson distribution in the limit $M_r >> \langle m \rangle_r$, and to the Bose-Einstein distribution for M_r=1.

Various analytic expressions for estimating M_r are published in the literature. Youmans and Hart[12] review a number of these, including Yura's simple r^{-2} approximation, which we apply here:[13]

$$M_r \approx 1 + \frac{Area_A \times A_{IFOV}}{\lambda^2\, r^2} \qquad \text{for } Area_{IFOV} \le Area_{RV}; \tag{7a}$$

$$M_r \approx 1 + \frac{Area_A \times A_{RV}}{\lambda^2\, r^2} \qquad \text{for } Area_{IFOV} > Area_{RV}. \tag{7b}$$

Youmans and Hart also present numerical techniques for calculating M_r, whose rigor exceed the level justified by our present purposes.

Assuming f/7 optics and shared use of the IR FPA's 5 cm aperture, a LADAR FPA with 30 µm pixels will have an 85.71 µrad IFOV. In Figure 5, the average number of photons received by a pixel is plotted versus range for three different pulse energies (4), assuming a 2% reflective target. Yura's approximation of the average number of speckle cells is overlaid (7). Together, these two parameters define the negative binomial distribution of primary photocarriers used below to compute target detection probability (6).

2. CHARACTERISTICS OF THE APD RECEIVER

A simplified picture of the optical portion of the engagement – the strength of the reflected signal and the statistics of its arrival – was presented in the preceding section. Although crude, this preliminary analysis is necessary to define plausible inputs for the detectors. We now address the detectors themselves.

2.1 Photocarrier generation

If the primary quantum efficiency of an APD's absorber is η, then the probability of creating a primary photoelectrons from m photons is:

$$P_{primaries}(a,m) = \eta^a\,(1-\eta)^{m-a}\,\frac{m!}{(m-a)!\,a!}, \tag{8}$$

where $m \ge a$, and the average number of electrons generated is just $\langle a \rangle_r = \eta \times \langle m \rangle_r$. As will be developed below, the probability of detecting a signal pulse depends upon the photoelectron yield from that pulse. To support this calculation, one must find the likelihood that a reflection

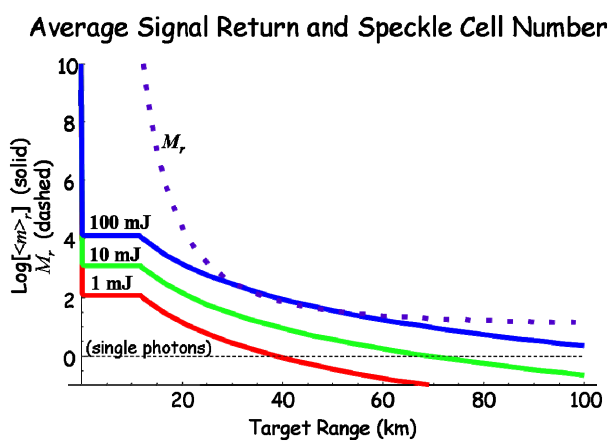

Figure 5: The average number of reflected photons received by a pixel is plotted for three laser pulse energies versus range (solid curves, logarithmic scale; eqn. 4). Yura's estimate of speckle cell number is overlaid (dashed curve, linear scale; eqn. 7).[13]

from a target at range r generates a primary photoelectrons. This result is obtained by summing (8) over (6):

$$P_{primaries}(a,r) = \sum_{m \geq a} P_{NB}(m,r) \times P_{primaries}(a,m) . \quad (9)$$

The absorption region is not a distinguishing feature that separates Geiger and Linear APDs, so the statistics of primary photocarrier generation are identical in both cases. At room temperature, the single-pass quantum efficiency through a 1 µm InGaAs absorber is 95% for 1064 nm light; it is only 0.13% for 1 µm of silicon.[14]

2.2 Detection of primary photocarriers

A Linear Mode APD can detect a weak signal if its internal multiplication gain is high enough to boost the signal photocurrent above the noise floor of the receiver's amplifier. The probabilistic nature of avalanche multiplication means that there is trial-to-trial variation of the linear gain experienced by individual primary photocarriers, so there is some uncertainty about the size of the output for a given input. The discrete statistical distribution of multiplied outputs (n) as a function of average gain (M), ionization coefficient ratio (k), and primary photocarrier inputs (a) was found by McIntyre and Conradi to be:[15,16]

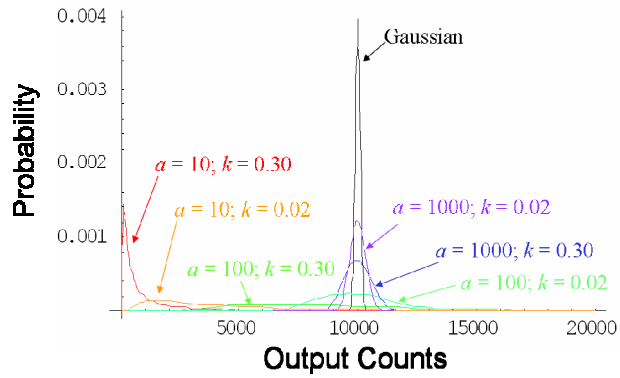

Figure 6: Comparison of Gaussian and McIntyre distributions for an average output of 10^4 electrons. The larger value of k is typical of III-V APDs; the smaller k is more typical of silicon. Note that for photon counting applications, a will be quite small (on the order of 1).

$$P_{McIntyre}(a,n) = \frac{a \times \Gamma\left(\frac{n}{1-k}+1\right)}{n \times (n-a)! \times \Gamma\left(\frac{n \times k}{1-k}+a+1\right)} \times \left(\frac{1+k(M-1)}{M}\right)^{a+\frac{n \times k}{1-k}} \times \left(\frac{(1-k)(M-1)}{M}\right)^{n-a} . \quad (10)$$

The McIntyre distribution is plotted in Figure 6 for some combinations of a and M that give an average output of n=10^4. It is seen that only the cases where a is large look like a Gaussian distribution; in the photon-counting regime, the most likely output of a Linear Mode APD is much smaller than the average output. The ionization coefficient ratio k also has a strong impact on the shape of the McIntyre distribution. Smaller values of k correspond to less feedback in the ionization process, and, hence, a smaller variance.

The probability that a given number of primary photocarriers (a) result in an amplified signal less than the receiver's threshold (n_{th}) is found by summing the McIntyre distribution between a and n_{th}. This is the chance that the pulse won't be detected. Since McIntyre's distribution is normalized, the probability that a primary carriers will be detected by a Linear Mode SPAD is just one minus this quantity:

$$P_L(a) = 1 - \sum_{n=a}^{n_{th}} P_{McIntyre}(a,n) . \quad (11)$$

In the trivial case where $a > n_{th}$, detection also occurs. The probability that an APD operated with an average gain of M=100 can detect a single primary photocarrier is plotted in Figure 7 as a function of amplifier noise threshold (n_{th}) for different values of k. Figure 7 highlights the critical role played by the ionization coefficient ratio (or, in engineered structures, it's effective value) in the Linear Mode detection problem.

In subsequent calculations, we have assumed k=0.02, M=250, and n_{th}=60 electrons, which give a single primary photocarrier detection probability of 50%. The ionization coefficient ratio k=0.02 is appropriate for conventional

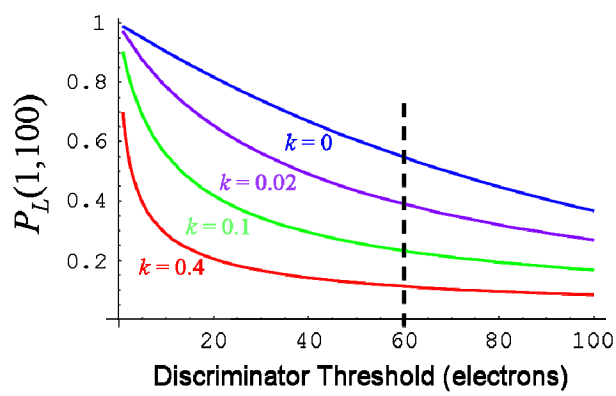

Figure 7: Probability of Linear Mode detection of a single primary photocarrier for M=100 as a function of the LADAR receiver's threshold setting, plotted for different values of k.

silicon APDs or highly engineered InGaAs-based APDs, and is somewhat worse than can be achieved with HgCdTe. The amplifier noise floor of n_{th}=60 electrons would give a factor of three margin for an ultra-low-noise amplifier with about 20 electrons RMS in-band noise, which can reasonably be achieved if low-capacitance bump-bonding is used to hybridize the detector pixel to its readout circuit.

One of the benefits of Linear Mode APD operation is that the threshold can be modified as a function of range, so as to increase the probability of detection while minimizing the false alarm rate. In our analysis, we increase the threshold value proportionally to $\sqrt{\langle a \rangle_r}$ for values above 60 electrons.

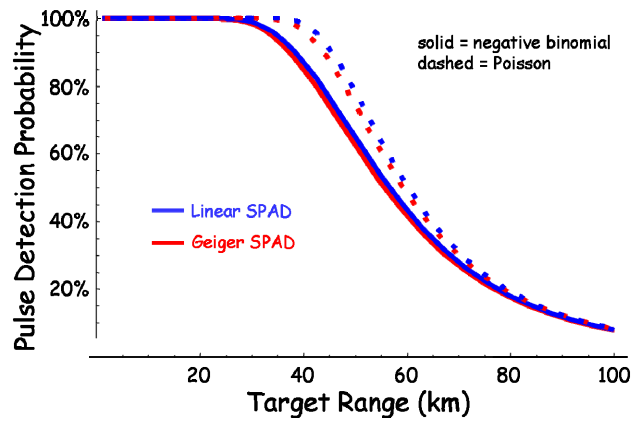

Figure 8: Probability of detecting the reflection of a 10 mJ laser pulse as a function of target range, for Linear (blue) and Geiger (red) SPADs characterized by a single primary photocarrier detection probability of 50%. Solid curves account for laser speckle and use the negative binomial distribution; dashed curves use Poisson statistics, and over-estimate detection probability at intermediate ranges.

The expression equivalent to (11) for Geiger SPADs is considerably simpler. At any given operating point above the breakdown voltage, the detector is characterized by the parameter P_{Br} which gives the probability that a single primary photocarrier injected into the multiplication layer of the APD will trigger avalanche breakdown. The current which flows in a SPAD in breakdown is unrelated to the number of primary carriers which triggered breakdown, so signal amplitude information is lost. However, because the breakdown current is quite large, it is trivial to measure. Consequently, the probability of detecting a primary carriers is simply one minus the probability that none of the carriers triggers breakdown:

$$P_G(a) = 1 - (1 - P_{Br})^a \,. \tag{12}$$

The junction breakdown probability P_{Br} is a function of operating conditions and device design, and trades with dark count rate.[17,18,19] To provide a uniform basis of comparison with the Linear APD in our model, we assume P_{Br}=50%.

The probability that a SPAD will detect a laser pulse reflected by a target at range r is found by summing the product of (9) with either (11) or (12), over a:

$$P_{PulseL}(r) = \sum_a P_{primaries}(a,r) \times P_L(a) \quad \text{(for Linear APDs);} \tag{13a}$$

$$P_{PulseG}(r) = \sum_a P_{primaries}(a,r) \times P_G(a) \quad \text{(for Geiger APDs).} \tag{13b}$$

As is illustrated in Figure 8, Linear SPADs have but a marginal advantage over Geiger SPADs when one only considers the probability of detecting the reflected signal. The missing ingredient is dark current, and its impact on the timing of pulse detection. The *pulse detection* probability plotted in Figure 8 is not the same thing as the *target detection* probability, because dark counts have not yet been treated. As we will develop, upset of Geiger Mode SPADs by dark counts severely limit their ability to observe long windows of time.

2.3 Importance of dark current and detector upset

For the purposes of this analysis, we have assumed SPADs with identical single photon detection efficiencies. Although the expressions for the detection probability of multi-carrier pulses, (11) and (12), are of different mathematical form, Figure 8 shows that the practical consequences of this distinction are negligible, absent timing considerations. We next address the aspect in which Linear and Geiger SPADs differ: their response to dark current.

An APD's dark current originates from several mechanisms. All reverse-biased diodes have 'saturation' or 'generation-recombination' (G-R) current that is associated with the minority carrier concentration in and near the junction; traps enhance the G-R leakage rate (the Shockley-Read-Hall process). Under strong reverse bias, band-to-band and trap-assisted tunneling dominates the dark current of a cooled APD.

Most G-R leakage originates in the absorber of an APD because the intrinsic carrier concentration is highest in the narrow-gap material from which the absorber is fabricated. G-R leakage is therefore a problem shared equally by both types of APD; it is mainly combated by cooling the device and using the widest-gap absorber alloy that will meet the quantum efficiency specification of the sensor. In contrast, the tunnel leakage mechanisms tend to be worse for Geiger SPADs than for Linear SPADs.

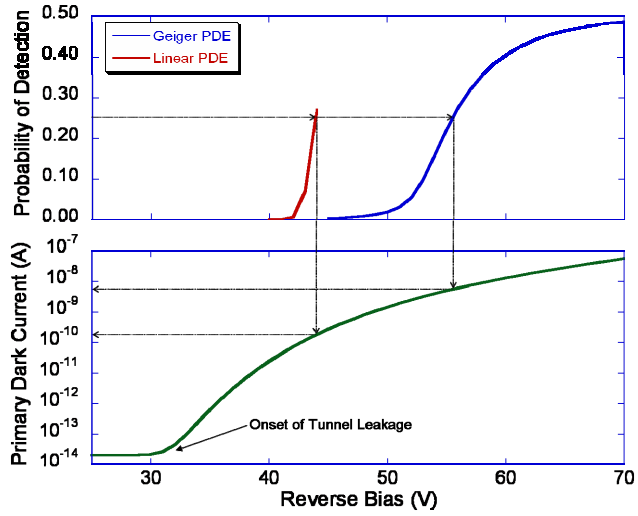

Figure 9: Relative primary dark current levels and single-carrier detection probabilities for Geiger and linear APDs estimated as a function of bias.

Leakage in a cooled APD is dominated by electric-field-dependent tunneling mechanisms. Since the same APD can be operated in either mode – and Geiger Mode operation requires higher bias – the primary dark current of any given APD in Geiger Mode is always higher than in Linear Mode. This point is illustrated in Figure 9, which attempts to estimate the primary dark current of a model InAlAs APD operated in both modes. Computational models of linear avalanche gain, multiplication noise, breakdown probability, and tunnel leakage versus electric field strength were combined with empirical measurements of dark current to make this estimate.[20,21] This figure should be regarded as illustrative rather than quantitative because the estimates of primary carrier detection efficiency are based on a multiplication noise more typical of silicon than InAlAs. In fact, no single APD structure is simultaneously optimized for both modes of operation. The point to be made is simply that for any particular structure, the leakage is always higher at higher bias, and Geiger Mode operation requires higher bias than Linear Mode operation.

Both Geiger and Linear Mode SPADs are vulnerable to dark current, but their response to it is very different. A Linear Mode SPAD will amplify primary dark current on the same basis as primary signal photocurrent, and can suffer spurious 'dark counts' as a result. Nonetheless, the act of 'counting' does not upset a Linear Mode SPAD – it can continuously read a string of valid and spurious counts without pause. In contrast, a Geiger SPAD must be reset following every breakdown event, and cannot be operated continuously. In order to reset a Geiger SPAD following breakdown, the bias must be lowered below breakdown, held in the quench state long enough for any traps in the junction to depopulate, and then the operating overbias must be applied again. The timing of this process varies depending upon other operating conditions such as temperature and the required voltage swing, but a typical quench time is 1 µs. Geiger Mode SPADs are blind during reset, so not only do they suffer dark counts – the dark counts can prevent them from observing valid target signals.

Cooling has an additional negative effect on Geiger APDs. The large current which flows through a Geiger APD during breakdown populates traps; cooling slows the rate at which these traps release their carriers, creating an extra source of dark current which persists after each detection event (Figure 10). Because the carriers released from the traps could trigger a spurious detection event, this 'afterpulsing' necessitates a delay following detection events that limits a Geiger APD's pulse pair resolution to perhaps a µs (300 m).

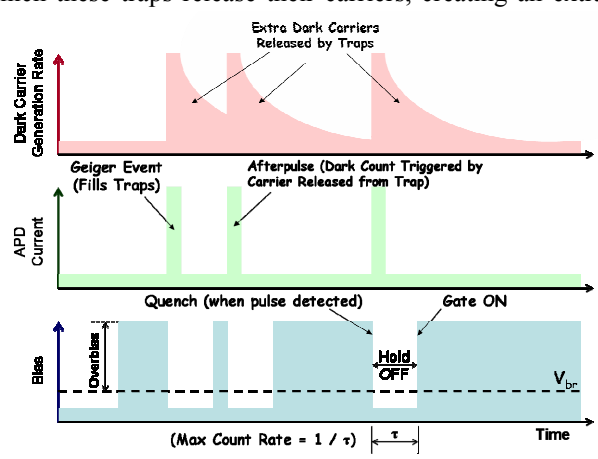

Figure 10: An illustration of gated operation of a Geiger SPAD, including afterpulsing.

In contrast, the current that flows during a Linear Mode detection event is too small to populate a significant number of traps, and so the pulse pair resolution of a Linear Mode SPAD is determined by the diode's junction transit time (ns-scale response and shorter rather than µs-scale response). Allowance for afterpulsing and the time required to quench a Geiger pulse means that whereas sub-nanosecond pulse pair resolution is a possibility with Linear SPADs, it is virtually impossible with a Geiger SPAD.

In general, dark current leakage and photogeneration from background light are statistically independent Poisson

processes, and their rates sum.[22] In the timing analysis that follows, we have chosen to include the noise contribution from background light with that from diode leakage and treat the total as a single generalized 'dark' current rate. This simplification avoids the necessity of estimating the background illumination explicitly.

The THAAD kill vehicle has a maximum speed of about 2.7 km s^{-1}, and RVs from theater and intercontinental missiles are estimated to travel at 5 and 7 km s^{-1} respectively, so the maximum closing velocity of the engagement should be less than 10 km s^{-1}. Two time scales are involved. The gate time (τ_{gate}) is the period during which the detector is active and able to detect a returning pulse. By one estimate, the standard deviation of the ground-based radar's range determination is at most 60 m.[11] A range gate spanning 240 m (i.e., ± 2σ) will have a better than 95% chance of containing the target. This corresponds to a gate time of τ_{gate} = 0.8 μs; 1 pA of dark current will generate an average of five primary dark electrons during this time.

The range bin time (τ_{bin}) is the smallest subdivision of time – and therefore the smallest distance resolution – that the LADAR system can register and record. Time bins of τ_{bin} =0.5 ns (7.5 cm resolution) – reflecting the full width at half maximum (FWHM) of the illuminating pulse – will be used for this calculation. The gate period is spanned by 1600 such bins, so the chance of a primary dark electron being generated by 1 pA of dark current during any given bin is 5/1600 = 0.3125%.

The main significance of τ_{gate} is that it is shorter than the recovery time of a Geiger SPAD (perhaps 1 μs). Consequently, if a dark count triggers a Geiger SPAD early in the gate period, the SPAD will be unable to record a real detection event if the pulse arrives later in τ_{gate}. This can be represented as a corrective factor for $P_{PulseG}(r)$ which we will refer to as F_{Geiger}. The probability that a dark count will obscure a pulse depends upon the rate of primary dark current and the timing of the pulse within τ_{gate}.

The average number of primary dark electrons generated per bin τ_{bin} just depends on the pixel's primary dark current I_{dark} according to:

$$\langle N_{dark} \rangle = \frac{I_{dark} \times \tau_{bin}}{q}. \tag{14}$$

This number plays a role similar to $\langle a \rangle_r$ in the earlier calculations, with the exception that $\langle N_{dark} \rangle$ doesn't change with target range or quantum efficiency. The primary dark electrons obey the Poisson distribution:

$$P_{Poisson}(N_{dark}) = \frac{\langle N_{dark} \rangle^{N_{dark}} \times \exp\left(-\langle N_{dark} \rangle\right)}{N_{dark}!}. \tag{15}$$

The probability of a dark count within any given range bin is therefore:

$$P_{DarkG} = \sum_{N_{dark}} P_{Poisson}(N_{dark}) \times P_G(N_{dark}). \tag{16}$$

Finally, the likelihood that the Geiger SPAD hasn't already been tripped by a dark count prior to bin B is just:

$$P_{ND}(B) = \left(1 - P_{DarkG}\right)^{B-1}. \tag{17}$$

To find the corrective pre-factor F_{Geiger}, one multiplies $P_{ND}(B)$ by the probability of the pulse arriving in each bin, and sums over the bins spanning the range gate.

The timing of pulse arrival within τ_{gate} is modeled as a Gaussian distribution around the center of the gate, using the range uncertainty of the ground-based radar for the standard deviation:

$$F_{Geiger} = \sum_B P_{ND}(B) \times \frac{1}{\sqrt{2\pi}\,\sigma} \int_{(B-1)\tau_{bin}}^{B\tau_{bin}} dt \exp\left[-\frac{\left(t - \frac{\tau_{gate}}{2}\right)^2}{2\sigma^2} \right]. \tag{18}$$

The Geiger pre-factor F_{Geiger} is plotted versus primary pixel dark current in Figure 11. For a 500 ns gate split into 0.5 ns bins, even 1 pA of dark current cuts the Geiger pulse detection probability by about 61% ($F_{Geiger} \approx 0.39$). Narrowing the range gate to less than ±2σ will reduce the probability of a spurious count interfering with pulse detection; however, the chance of missing the pulse altogether will rise. Therefore, for any given level of primary dark current, there is an optimal range gate, which considers both the probability of the range-gate containing the target of interest, and the probability that the Geiger SPAD won't have already triggered off of dark current by the time the pulse arrives. As shown in Figure 12, for 10 pA of primary dark current, the optimal gate time is found to be about 135 ns, with a maximum possible correction factor of $F_{Geiger} = 0.0618$.

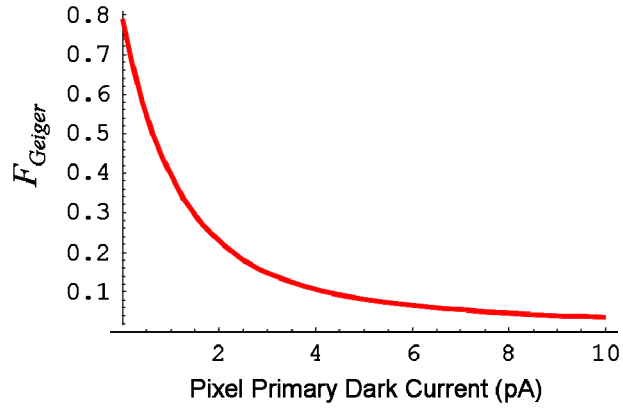

Figure 11: The Geiger pre-factor plotted as a function of primary dark current for a 500 ns gate time.

No similar correction factor is required for a Linear SPAD, as Linear APDs are not susceptible to upset. A further advantage enjoyed by Linear Mode APDs is the possibility of ignoring dark current by means of a variable threshold. Initially a minimum n_{th} value is imposed by the noise floor of the receiver's amplifier. When the target is at extreme range and the signal is weak, a minimum threshold is required in order to detect the signal with a Linear Mode SPAD. In this condition, the SPAD is maximally susceptible to dark counts. However, when the target gets closer and the reflected signal is strong, the primary photocarrier generation rate will be substantially higher than the primary dark current, and it should be possible to reject the amplified dark current without losing the amplified signal. This can improve the image quality of a Linear Mode SPAD-based LADAR FPA in the vital terminal guidance phase.

The probability of a Geiger APD registering a dark count (P_{DarkG}) was calculated above. By analogy to the methods for computing detection of a pulse, the dark count probability for a Linear Mode SPAD is:

$$P_{DarkL} = \sum_{N_{dark}} P_{Poisson}(N_{dark}) \times P_L(N_{dark}) \,. \tag{19}$$

where N_{dark} has been substituted for the primary carrier count a. The variable threshold is found in $P_L(N_{dark})$, defined in (11).

3. TARGET DETECTION PROBABILITIES

Having allowed for the possibility of detector upset by spurious counts, we now return to the issue of the noise they introduce. If the LADAR was observing a stationary target, one could identify valid returns by their accumulation in a single range bin. Although a 10 km s^{-1} target will only move 1 m during the time between pulses from a 10 kHz illuminating laser, that's much larger than the 15 cm increment corresponding to a 0.5 ns range bin. Consequently, consecutive returns off a single target will not register in a single range bin. Nonetheless, we will treat the problem as if the statistics of a single range bin are meaningful. If the target's closing velocity is known within a reasonable tolerance based on data from ground-based radar, a suitable algorithm can sort through the LADAR data and identify correlations between hits in adjacent range bins. In that

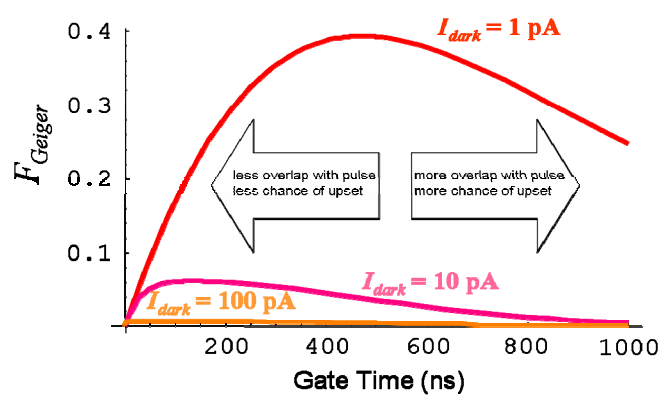

Figure 12: The Geiger pre-factor plotted as a function of gate time for different primary dark current levels; optimal gate time is a tradeoff between overlap with the reflected pulse and chance of upset by dark current.

way, data from different range bins can be analyzed as though it represents a single 'moving' range bin.

We will compute the LADAR's target detection probability based on the requirement of receiving three times as many valid digital hits as dark counts out of a number of consecutive frames. We will explicitly calculate the case for 128 bins, but the math is general.

To estimate target detection probability, we will assume that the closing velocity of the target is 10 km s^{-1}, and that data is processed in batches of 128 pulses (covering 127 m). Target detection probability at range r will be based on the likelihood that signal hits exceed dark counts by a factor of 3 (SNR = 3) for the pulses between r and r + 127 m.

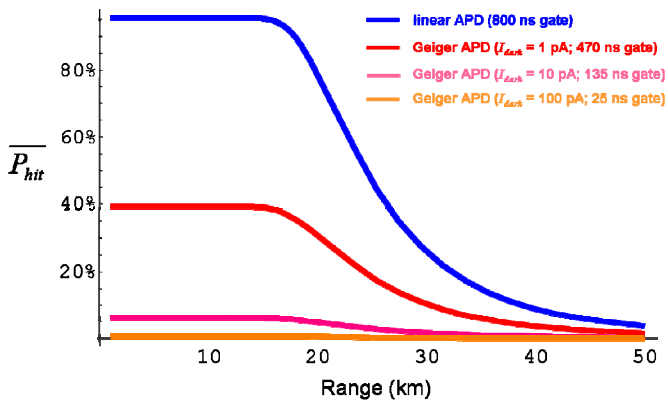

Figure 13: Pulse detection probability averaged over 128 range bins, taking finite gate time and Geiger APD upset into account for I_{dark} = 10 pA.

The probability of getting i dark counts in j pulses, with a uniform dark count probability P_{Dark} given by either (16) or (19) is:

$$P_{noise}(i,j) = P_{Dark}^{i} \times (1 - P_{Dark})^{j-i} \times \frac{j!}{(j-i)! \times i!}. \tag{20}$$

The alert reader will note that P_{DarkL} is not independent of range for the case of a dynamically adjusted discriminator threshold. However, dynamic thresholding only applies to the endgame when there is an abundance of reflected signal photons, and the target detection probability has already saturated.

Finding the probability of getting s valid hits is much more difficult to calculate exactly because the probability of a detection event (P_{hit}) varies with range – P_{hit} is either (13a) or (13b) modified by (18). Technically, for every value of s, the individual probability of every possible permutation of s hits must be totaled, and each permutation has a different probability. Noting that P_{hit} changes by at most 2% in any 127 m span, we elect to use a single value of P_{hit} that is its average over the span between r and r + 127 m. Figure 13 shows $\overline{P_{hit}}$ plotted versus range for both types of detector and three different dark current levels; an 800 ns gate was used for the Linear SPAD calculation, but optimal gate times of 470 ns, 135 ns, and 25 ns were used for primary pixel dark current levels of 1 pA, 10 pA, and 100 pA for the Geiger SPAD. With this approximation:

$$P_{signal}(s,j) \cong \overline{P_{hit}}^{\,s} \times (1 - \overline{P_{hit}})^{j-s} \times \frac{j!}{(j-s)! \times s!}. \tag{21}$$

The overlap of these two distributions at any given range determines the detection probability at that range.

The detection probability is constructed from $P_{noise}(i,j)$ and $P_{signal}(s,j)$ by adding cases for $0 \le i \le Q/3$, where Q is the number of pulses to be correlated (128 in this case). For each value of i, the probability of obtaining i dark counts is multiplied by the probability that $s \ge 3i$. When Q is not an integer multiple of 3 (or the desired signal-to-noise ratio), one rounds down:

$$P_{Detect} = \sum_{i=0}^{i=Q/3} P(i,Q) \times \sum_{s=3i}^{s=Q} P(s,Q). \tag{22}$$

Target detection probability is plotted in Figure 14.

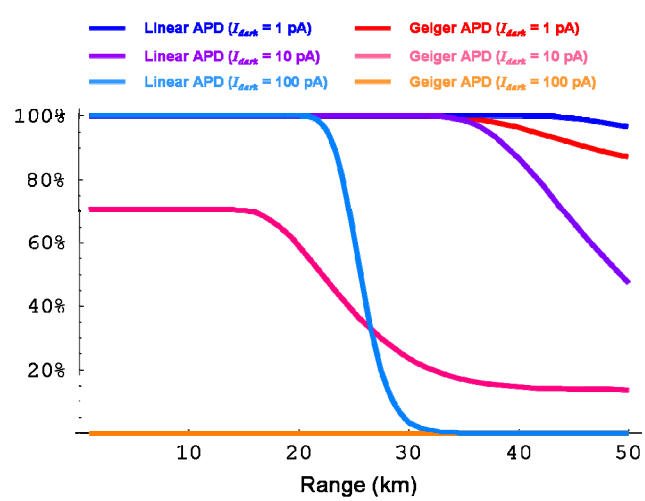

Figure 14: Target detection probability (probability of better than 3 times as many valid hits as dark counts, in 128 pulses) for linear and Geiger SPAD pixels calculated versus target range for several different primary dark current levels.

4. SUMMARY

Strapdown LADAR seekers must perform precise target detection, tracking, and aimpoint imaging in the presence of shock and vibration. Solid-state APDs are a rugged, fully monolithic detector technology that is well-suited to this task. Expressions for the probabilities of detection, false event creation, and pixel drop-out have been found for both Geiger and linear mode SPADs assuming various detector performance characteristics and operational scenarios.

In the past, Geiger SPADs have been preferred for tasks requiring sensitivity to single photons. However, LADAR seekers based on Geiger APDs achieve single photon sensitivity at the price of high dark current and long deadtimes. Moreover, Geiger APDs cannot resolve signal amplitude nor can their response be thresholded to reject spurious dark count events. In contrast, linear SPADs are superior in every regard – if a combination of detector and amplifier can be engineered to compete with Geiger APDs on sensitivity. Recent advances in low-noise amplifier design and techniques for suppressing APD multiplication noise have brought photon counting within reach of linear APD systems.

Most of the advantage linear SPADs have over Geiger SPADs stems from insensitivity to upset. In addition to the substantial limit on Geiger SPAD pulse detection probability imposed by dark current, sensitivity to upset can also prevent imaging inside threat clouds. Reflected laser energy from objects in the foreground can act to conceal targets deeper in the threat cloud because Geiger SPADs which trigger on the initial return will not be active when the photons that were reflected from the target arrive. If multiple targets are within the IFOV of a single pixel, only a linear SPAD will be able to see both. In general more laser pulses and range gate manipulation will be needed to map a threat cloud with a Geiger SPAD than with a linear SPAD of equivalent sensitivity.

Linear SPADs can sense signal amplitude, which is a valuable piece of information for target discrimination; Geiger SPADs cannot. Linear SPADs intrinsically have lower primary dark current than Geiger SPADs of the same design, and they can employ thresholding techniques to reject dark current when they receive multi-photon signals; Geiger SPADs cannot. Finally, the speed of a Linear SPAD is limited by carrier dynamics rather than external biasing considerations, so Linear SPADs are capable of sub-nanosecond pulse pair resolution; Geiger SPADs are not.

Nevertheless, today Geiger SPADs are the more mature technology. Geiger SPADs have been tested in 3-D LADAR applications, whereas Linear SPAD FPAs are just emerging. At this date, the shortcomings of Geiger SPADs with respect to upset and timing are clear, and adequately represented by our modeling – what remains to be demonstrated is the ability of Linear SPADs to meet their potential.

REFERENCES

1 M. E. DeFlumere, M. W. Fong and H. M. Stewart "Dual Mode (MWIR AND LADAR) Seeker for Missile Defense"ADM201460. *11th Annual AIAA/MDA Technology Conference,* July 2002, Monterey, CA.,

2 R. Heinrichs, B. Aull, R. Marino, D. Fouche, A. McIntosh, J. Zayhowski, T. Stephens, M. O'Brien, and M. Albota, "Three-dimensional laser radar with APD arrays," *Laser Radar Technology and Applications VI*, G. W. Kamerman, ed., Proc. SPIE vol. 4377, pp. 106–117 (2001).

3 J. Boisvert, G. Kinsey, D. McAlister, T. Isshiki, R. Sudharsanan, and M. Krainak, "Large area AlAs_InGaAs single photon counting avalanche photodiodes," *Laser Radar Technology and Applications IX*, G. W. Kamerman, ed., Proc. SPIE vol. 5412, pp. 126–136 (2004).

4 L. LaCroix and S. Kurzius, "Peeling the Onion An Heuristic Overview of Hit-to-Kill Missile Defense in the 21st Century," *Quantum Sensing and Nanophotonic Devices II*, M. Razeghi, G. J. Brown, ed., Proc. SPIE vol. 5732

5 J. Barenz, R. Baumann, and H.D. Tholl, "Eyesafe Imaging LADAR/Infrared Seeker Technologies," *Laser Radar Technology and Applications X*, G. W. Kamerman, ed., Proc. SPIE vol. 5791 (SPIE, Bellingham, WA, 2005)

6 H. Yingbo and Q. Yong, "THAAD-Like High Altitude Theater Missile Defense: Strategic Defense Capability and Certain Countermeasures Analysis," *Science and Global Security*, no. 11, pp.151-202 (2003).

7 A. M. Sessler et al., *Countermeasures: A Technical Evaluation of the Operational Effectiveness of the Planned U.S. National Missile Defense System* (MIT Security Studies Program, Cambridge, MA), 2000.

8 D. G. Fouche, B. F. Aull, M. A. Albota, R. M. Heinrichs, J. J. Zayhowski, M. E. O'Brien and R. M. Marino, "Three-Dimensional Imaging Laser Radar Using Microchip Lasers and Geiger-Mode Avalanche July 2000.

9 J. Beck, C. Wan, M. Ohlson, M. Kinch, and J. Robinson, "Progress in HgCdTe Electron Avalanche Photodiode Development," *2003 Military Sensing Symposia Specialty Group Meeting on Infrared Detectors*, 24-28 February 2003.

10 K. Vaccaro et al., "Evaluation of InGaAs/InAlAs-based APDs as Photon Counters," February 2005

11 T. B. Cochran, W. M. Arkin, and M. M. Hoenig, *Nuclear Weapons Databook, Volume I: U.S. Nuclear Forces and Capabilities* (Cambridge, MA: Ballinger, 1984), 75.
12 D. G. Youmans and G. A. Hart, "Numerical evaluation of the 'M' parameter for direct detection ladar," *SPIE Proceeding*, vol. 3380: *Laser Radar Technology and Applications III*, April 1998.
13 H. T. Yura, "LADAR detection statistics in the presence of pointing errors," *Applied Optics*, vol. 33, no. 27, p. 6482 (1994).
14 S. Adachi, Optical Constants of Crystalline and Amorphous Semiconductors – Numerical Data and Graphical Information, (Boston: Kluwer Academic Publishers, 1999), pp. 29 & 362.
15 R. J. McIntyre, "The distribution of gains in uniformly multiplying avalanche photodiodes: Theory," *IEEE Transactions on Electron Devices*, vol. ED-19, pp. 703-713 (1972).
16 J. Conradi, "The distribution of gains in uniformly multiplying avalanche photodiodes: Experimental," *IEEE Transactions on Electron Devices, vol. ED-19*, pp. 713-718 (1972).
17 D. A. Ramirez, M. M. Hayat, G. Karve, J. C. Campbell, S. N. Torres, B. E. A. Saleh, and M. C. Teich, "Detection efficiencies and generalized breakdown probabilities for nanosecond-gated near infrared single-photon avalanche photodiodes," *IEEE Journal of Quantum Electronics*, vol. 42, no. 2, pp. 137-145 (2006).
18 M. M. Hayat, U. Sakoglu, O.-H. Kwon, S. Wang, J. C. Campbell, B. E. A. Saleh, and M. C. Teich, "Breakdown probabilities for thin heterostructure avalanche photodiodes," *IEEE Journal of Quantum Electronics*, vol. 39, no. 1, pp. 179-185 (2003).
19 M. A. Saleh, M. M. Hayat, O.-H. Kwon, A. L. Holmes, Jr., J. C. Campbell, B. E. A. Saleh, and M. C. Teich, "Breakdown voltage in thin III-V avalanche photodiodes," *Applied Physics Letters*, vol. 79, no. 24, pp. 4037-4039 (2001).
20 G. Karve, S. Wang, F. Ma, X. Li, J. C. Campbell, R. G. Ispasoiu, D. S. Bethune, W. P. Risk, G. S. Kinsey, J. C. Boisvert, T. D. Isshiki, and R. Sudharsanan, "Origin of dark counts in $In_{0.53}Ga_{0.47}As/In_{0.52}Al_{0.48}As$ avalanche photodiodes operated in Geiger Mode," *Applied Physics Letters*, vol. 86, 063505 (2005).
21 M. A. Saleh, M. M. Hayat, O. Kwon, A. L. Holmes, Jr., J. C. Campbell, B. E. A. Saleh, and M. C. Teich, "Breakdown voltage in thin III-V avalanche photodiodes," *Applied Physics Letters*, vol. 79, no. 24, pp. 4307-4309 (2001).
22 D. G. Fouche, "Detection and false-alarm probabilities for laser radars that use Geiger-mode detectors," Applied Optics, vol. 42, no. 27, pp. 5388-5398 (2003).